Surface superconductor-insulator transition induced by electric field

Liyu Yin,[1] Yunfei Bai,[1] Ming Zhang,[1] A. A. Shanenko,[2] and Yajiang Chen [1,*]

[1]*Key Laboratory of Optical Field Manipulation of Zhejiang Province, Department of Physics,*
Zhejiang Sci-Tech University, Zhejiang 310018, China
[2]*HSE University, 101000 Moscow, Russia*

It is well known that the electric field can induce phase transitions between superconducting, metallic and insulating states in thin-film materials due to its control of the charge carrier density. Since a similar effect on the charge carriers can also be expected for surfaces of bulk samples, here, we investigate the transformation of the surface states in a superconductor under an applied screened electric field. Our study is performed by numerically solving the self-consistent Bogoliubov–de Gennes equations for the one-dimensional attractive Hubbard model. It is found that the surface insulating regime occurs at sufficiently large (but still experimentally accessible) electric fields. Our calculations yield the phase diagram of the surface superconducting, metallic, and insulating states for a wide range of temperatures and applied fields. Our results are in qualitative agreement with the phase diagram obtained with the transport measurements for (Li, Fe)OHFeSe thin flakes [Ma *et al.*, Sci. Bull. **64**, 653 (2019); Yin *et al.*, ACS Nano **14**, 7513 (2020)].

DOI: 10.1103/PhysRevB.108.054508

I. INTRODUCTION

Due to the capability of modulating the carrier concentration, the electric field has been utilized as one of the most important experimental tools in the field of superconductivity for several decades [1–7]. In particular, electric-field effects on the superconductor-metal transition have been revealed theoretically and experimentally. Electrostatic charging created by an external electric field ($E \approx 2^{-7}$ V/m) is able to cause a shift of the superconducting transition temperature ($\Delta T_c \approx 10^{-5}$ K) in both tin and indium thin films [1,2]. Electric fields change the energy of itinerant electrons in atomically thin flakes of $NbSe_2$, which results in shifting the chemical potential and changing the density of states in the Debye window and, in turn, altering T_c [8]. Although electrons are heavily affected by an electric field near surfaces, it has been shown by electrical and thermal conductivity measurements that tin films possess no surface superconductivity in the presence of an electric field [3]. However, for systems with a sufficiently low Fermi level, the surface bound states of electrons induced by electric fields may result in the appearance of multigap surface superconductivity [9]. In addition, T_c of oxide superconductors (e.g., 8-nm-thick $GdBa_2Cu_3O_{7-x}$ films, Nb-doped $SrTiO_3$ films) can be tuned by sufficiently large electric fields due to dielectric breakdown [10–12]. Furthermore, the electric field influences other superconducting properties related to the superconductor-metal transition, e.g., suppression of the critical supercurrent [4,5,13–16].

Electric fields can also induce a superconducting state in insulators. For example, with gate voltage V_g increasing from 0 to 42.5 V, the resistance of a 10.22-Å-thick amorphous Sb film at $T = 65$ mK [17] drops continuously from 22 to 0 kΩ, which implies that the sample may undergo the insulator-metal and metal-superconductor transitions in sequence. Here, the electric field associated with the onset of superconductivity is sufficiently high (up to 4.2×10^{10} V/m), corresponding to the dielectric breakdown. It was found that increasing electron concentrations screens the electron-electron interactions, which produces an effective attractive potential and promotes the superconductive correlations. More particularly, for a pristine $SrTiO_3$ channel with a size of $15 \times 200\,\mu m^2$ [18], the system undergoes a sharp superconducting transition with a midpoint critical temperature $T_c^{mid} = 0.4$ K at $V_g = 3$ V according to transport measurements. In this case, the electric field is 2–3 orders of magnitude weaker than the dielectric breakdown field [19], and the sample is metallic at $T < 0.1$ K and $V_g = 2.50$ V because its resistance is about $20\,\Omega$. This means that this transition actually occurs from the metallic state to the superconducting state as the electric field increases. Similar transitions have also been observed in 2-nm-thick $GdBa_2Cu_3O_{7-x}$ films [11], atomically flat ZrNCl films [20], $La_{2-x}Sr_xCuO_4$ films [21], etc.

Recently, transport measurements revealed [22,23] the direct superconductor-insulator transition that occurs in thin (Li, Fe)OHFeSe flakes with $T \approx 0$ and $V_g \approx 5.13$ V. Its mechanism is not clear yet, as many important details, such as the differential conductance dI/dV and the T-dependent resistance, are missing. However, this is certainly an example where the electric-field effects play a crucial role.

In the present work, motivated by these experiments with thin (Li, Fe)OHFeSe flakes [22,23], we investigate the transformation of the surface properties in a bulk superconductor under an applied electric field. In particular, we consider the effect of a screened electric field on the superconducting state near the edges of the system within the

*yjchen@zstu.edu.cn

one-dimensional attractive Hubbard model at the half-filling level by numerically solving the self-consistent Bogoliubov–de Gennes (BdG) equations. Our study demonstrates that the direct surface superconductor-insulator transition does arise in the superconductor for sufficiently strong electric fields and low temperatures. Moreover, our findings are in qualitative agreement with the phase diagram obtained by the transport measurements for (Li, Fe)OHFeSe thin flakes [22,23].

The present paper is organized as follows. In Sec. II we discuss the BdG equations for the one-dimensional attractive Hubbard model in the presence of an applied (screened) electric field. In our study the BdG equations are solved numerically, in a self-consistent manner, and the main points of this procedure are also outlined in Sec. II. In Sec. III, we consider numerical results for the pair potential and electron distribution together with the corresponding quasiparticle energies and wave functions. These results yield the phase diagram of the surface superconducting, metallic, and insulating states versus the temperature and the electric-field strength. Finally, our main conclusions are given in Sec. IV.

II. THEORETICAL FORMALISM

A. Bogoliubov–de Gennes equations

As we are interested in the qualitative picture of the surface-state transformations, our analysis can be simplified by considering a one-dimensional chain of atoms in a parallel electric field. The corresponding attractive Hubbard model with s-wave pairing within the tight-binding approximation is based on the grand-canonical Hamiltonian [24,25]:

$$\mathcal{H} - \mu \mathcal{N}_e = -\sum_{i\delta\sigma} t_\delta c_{i+\delta,\sigma}^\dagger c_{i\sigma} + \sum_{i\sigma} [V(i) - \mu] n_{i\sigma} - g \sum_i n_{i\uparrow} n_{i\downarrow}, \tag{1}$$

where μ is the chemical potential and $\mathcal{N}_e$ is the total electron number operator, i.e., $\mathcal{N}_e = \sum_{i\sigma} n_{i\sigma} = \sum_{i\delta} c_{i\sigma}^\dagger c_{i\sigma}$, with $c_{i\sigma}$ ($c_{i\sigma}^\dagger$) being the annihilation (creation) operator of an electron with spin σ ($=\uparrow, \downarrow$) at sites $i = 0, \dots, N + 1$. t_δ is the hopping rate of electrons between sites i and $i + \delta$. In the present study only the nearest neighbors are taken into account, i.e., $\delta = \pm 1$, and thus, we have $t_\delta = t$. Finally, g denotes the on-site attractive interaction between electrons resulting from the electron-phonon coupling, and $V(i)$ is the electrostatic energy appearing due to the presence of a screened electric field.

Within the mean-field approximation one gets the effective Hamiltonian [26]

$$H_{\text{eff}} = -t \sum_{i\delta\sigma} c_{i+\delta,\sigma}^\dagger c_{i\sigma} + \sum_{i\sigma} [V(i) - \mu] n_{i\sigma} - \sum_i [\Delta(i) c_{i\uparrow}^\dagger c_{i\downarrow}^\dagger + \Delta^*(i) c_{i\downarrow} c_{i\uparrow}], \tag{2}$$

with $\Delta(i)$ being the site-dependent superconducting pair potential. Diagonalizing H_{eff} through the generalized

Bogoliubov-Valatin transformation [26], we obtain the BdG equations [27–30]

$$\epsilon_\alpha u_\alpha(i) = \sum_{i'} H_{ii'} u_\alpha(i') + \Delta(i) v_\alpha(i), \tag{3a}$$

$$\epsilon_\alpha v_\alpha(i) = \Delta^*(i) u_\alpha(i) - \sum_{i'} H_{ii'}^* v_\alpha(i'), \tag{3b}$$

where $H_{ii'}$ is the single-particle Hamiltonian and ϵ_α, $u_\alpha(i)$, and $v_\alpha(i)$ are the energy and wave functions of quasiparticles, respectively. The index α enumerates the quasiparticle states in energy ascending order (only the states with positive quasiparticle energies are taken into consideration) [31,32]. We apply open boundary conditions; that is, the quasiparticle wave functions vanish at $i = 0$ and $N + 1$. The Hartree-Fock potential is ignored in our study since its main effect is barely shifting the chemical potential [33]. The single-particle Hamiltonian $H_{ii'}$ is of the form

$$H_{ii'} = -t \sum_{\delta=\pm 1} \delta_{i',i+\delta} + [V(i) - \mu] \delta_{ii'}, \tag{4}$$

where the chemical potential μ is determined by the electron-filling level $\bar{n}_e = \sum_i n_e(i)/N$, where the electron distribution $n_e(i)$ is as follows:

$$n_e(i) = 2 \sum_\alpha [f_\alpha |u_\alpha(i)|^2 + (1 - f_\alpha) |v_\alpha(i)|^2], \tag{5}$$

with $f_\alpha = f(\epsilon_\alpha)$ being the Fermi-Dirac distribution. Below we focus on the half-filling case, i.e., $\bar{n}_e = 1$. The spatial pair potential $\Delta(i)$ is related to the quasiparticle energies and wave functions by [29,30,34]

$$\Delta(i) = g \sum_\alpha u_\alpha(i) v_\alpha^*(i) [1 - 2f_\alpha]. \tag{6}$$

Here, the sum is over the quasiparticle states within the Debye window, i.e., $0 \leqslant \epsilon_\alpha \leqslant \hbar\omega_D$, where ω_D is the Debye frequency.

The BdG equations (3) are solved self-consistently together with Eqs. (5) and (6). First, we solve the BdG equations using some initial guess for the chemical potential μ and pair potential $\Delta(i)$. Second, based on this solution, we find the electron-filling level and the new pair potential according to Eqs. (5) and (6), respectively. Third, if the new pair potential differs significantly from the initial guess and/or the electron-filling level is lower or higher than the half-filling one, we go back to the first step, replacing the initial guess for the pair potential by its new variant and slightly changing the chemical potential. The procedure is repeated until the convergence of $\Delta(i)$ under the condition that $\bar{n}_e$ approaches the half-filling level.

B. Screened electric field E(x) and electrostatic energy V(x)

The parallel electric field is introduced by using the approach of two charge reservoirs with equal but opposite charges located at the opposite surfaces of the system [19]. Instead of a uniform electric field appropriate for insulating materials [25,35], here, we consider a screened electric field. This variant is relevant for the case when the bulk of the sample is metallic or superconductive. Then, following Ref. [16],

the electric field is written as

$$\mathbf{E}(x) = E_0[e^{-x/\lambda_E} + e^{-(L-x)/\lambda_E}]\hat{\mathbf{x}}$$
$$= 2\,E_0\,e^{-L/2\lambda_E}\cosh[(2x-L)/2\lambda_E]\hat{\mathbf{x}}, \qquad (7)$$

where λ_E is the screening length; E_0 is the value of the electric field at the boundaries; L is the chain length, i.e., $L = (N+1)a$, with a being the lattice constant; $x = (i-1)a$ is the site coordinate; and $\hat{\mathbf{x}}$ is the unit vector along the chain.

The screening of the electric field in the presence of the superconductor-metal-insulator surface transformation is a rather complex problem [16,36–40]. In the literature, two simplified approximate relations for λ_E are often employed: one is the Thomas-Fermi approximation [1,36], which can be useful for low temperatures, and the other is the Debye approximation [36–38], which can be used for sufficiently high temperatures. There are also phenomenological approaches when λ_E is considered a calculation parameter. For example, λ_E was set to 1 nm in Refs. [16,37,38], and it was chosen to be equal to the lattice constant in Ref. [38].

Below we adopt the phenomenological variant, and the screening length is chosen to be the Fermi wavelength times the numerical factor γ, i.e.,

$$\lambda_E = \gamma \lambda_F, \qquad (8)$$

where γ is a parameter of our calculations and λ_F is usually of the order of the lattice constant. Due to its phenomenological character, our approach does not give any details about γ. We adopt $\gamma = 2$, keeping in mind that our qualitative results are not sensitive to the particular choice of this parameter.

To estimate λ_F, we employ the single-particle dispersion relation [24] of the one-dimensional (1D) Hubbard model in the absence of the electric field $\xi_k = -2t\cos(ka) - \mu$. Keeping the first two terms in the expansion of ξ_k in ka, we obtain

$$\xi_k \approx \xi_s + \frac{\hbar^2 k^2}{2m_e} - \mu, \qquad (9)$$

with $\xi_s = -2t$ and the effective electron band mass $m_e = \hbar^2/2ta^2$. Then, the Fermi wave number is obtained from $\xi_{k_F} = 0$ as $k_F = \sqrt{(\mu - \xi_s)/ta^2}$, and the Fermi wavelength $\lambda_F = 2\pi/k_F$ is given by

$$\lambda_F = 2\pi a\sqrt{\frac{t}{\mu - \xi_s}} = \sqrt{2}\pi a, \qquad (10)$$

where for the half-filling case we use $\mu = 0$.

According to the relation $\mathbf{E}(x) = -\frac{d[V(x)/q]}{dx}\hat{\mathbf{x}}$, with $q = -e$ being the electron charge, we obtain the following expression for $V(x)$:

$$V(x) = -2\,q\lambda_E\,E_0\,e^{-L/2\lambda_E}\sinh[(2x-L)/2\lambda_E]. \qquad (11)$$

In our calculations, the energy, length, and electric field are in units of the hopping rate t, the lattice constant a, and t/ea, respectively.
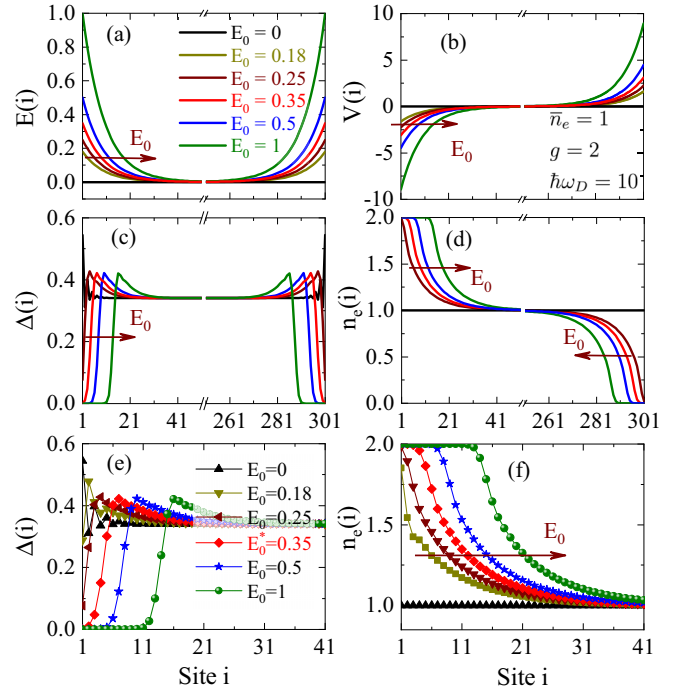
FIG. 1. (a) The screened electric field $E(i)$, (b) the electronic potential energy $V(i)$, (c) the pair potential (order parameter) $\Delta(i)$, and (d) the spatial electron distribution $n_e(i)$ calculated for $E_0 = 0$, 0.18, 0.25, 0.35, 0.5, and 1. (e) and (f) Zoomed-in plots of $\Delta(i)$ and $n_e(i)$ near the left chain edge. The calculations are done at $T = 0$ for the material parameters $\bar{n}_e = 1$, $g = 2$, $\hbar\omega_D = 10$, $N = 301$, and $\gamma = 2$. The energy-related quantities $\Delta(i)$, $V(i)$, g, and $\hbar\omega_D$ are given in units of the hopping rate t, while E_0 is in units of t/ea, with a being the lattice constant.

III. RESULTS AND DISCUSSION

A. Surface insulating states of superconductors induced by an electric field at $T = 0$

Figure 1 shows a typical example of the surface superconductor-insulator transition induced by a screened electric field $E(i)$ in a one-dimensional superconducting chain with $N = 301$ and $E_0 = 0$, 0.18, 0.25, 0.35, 0.5, and 1 in the half-filling case at $T = 0$. Here, the screening length λ_E is equal to 9.0 (as $\lambda_F = 4.5$). The coupling constant g is set to 2, and $\hbar\omega_D = 10$.

The electrostatic field $E(i)$ and the corresponding potential energy $V(i)$ are shown in Figs. 1(a) and 1(b). As can be seen, $E(i)$ drops from E_0 at the edges to zero in the center of the chain, while $V(i)$ sharply increases with i in the vicinity of the boundaries, according to Eqs. (7) and (11). The corresponding spatial distribution of the pair potential is given by Fig. 1(c). We can see that $\Delta(i)$ is nearly uniform in the center of the chain, but when approaching an edge (both left and right), it exhibits a peak with a subsequent abrupt drop to zero. From the zoomed-in image in Fig. 1(e), we learn that the peaks in $\Delta(i)$ shift towards the center of the chain with increasing E_0. When E_0 crosses the critical value $E_0^* = 0.35$, $\Delta(i = 1)$ vanishes. Then, this zero-pair-potential region expands with a further increase in E_0, so that one finds that $\Delta(i \leqslant 11) = 0$ for
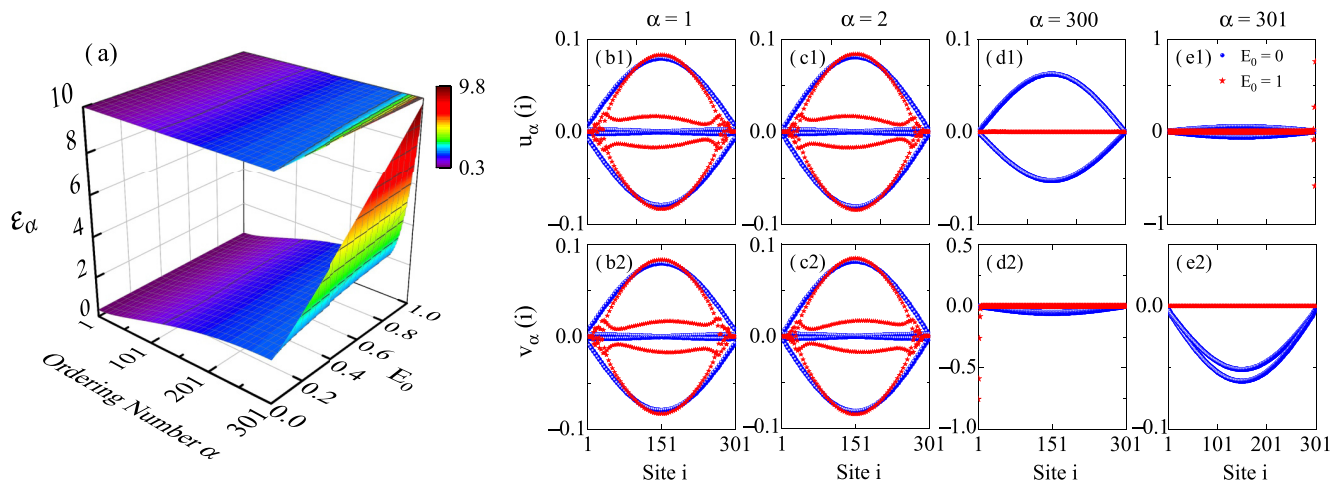
FIG. 2. (a) The quasiparticle energy ϵ_α (in units of t) as a function of the quantum (ordering) number α and the boundary electric field E_0; here, the upper panel represents the contour plot of ϵ_α. (b1) and (b2) The quasiparticle wave functions $u_\alpha(i)$ and $v_\alpha(i)$ versus the site number i at $\alpha = 1$; the same quantities, but for $\alpha = 2$, 300, and 301, are shown in (c1) and (c2), (d1) and (d2), and (e1) and (e2), respectively. In (b)–(e) the blue points correspond to the case of zero field, whereas the red ones are for $E_0 = 1$. The material parameters are the same as in Fig. 1.

$E_0 = 1$. The same happens near the opposite edge, where we have $\Delta(i \geqslant 291) = 0$.

Now, we turn to the electron distribution. In the absence of the electric field, $n_e(i)$ is uniform and given by the uniform black line in Fig. 1(d) and the black line with the upward triangles in the zoomed-in image in Fig. 1(f). The character of the distribution changes in the presence of the applied field. Indeed, for $E_0 > 0$ one finds that $n_e(i)$ exhibits a significant increase near the left edge and a decrease near the right edge. In the center of the chain $n_e(i)$ approaches the half-filling value. When E_0 crosses $E_0^* = 0.35$, site $i = 1$ becomes fully occupied (see the red curve with diamonds), i.e., $n_e(i = 1) = 2$, which corresponds to the onset of the surface insulating state. At the same time $n_e(i = 301) = 0$, which also corresponds to the onset of the insulating state at the right edge. Thus, E_0^* can be referred to as the critical electric field of the surface superconductor-insulator transition. For $E_0 > E_0^*$, the surface insulating state expands. For example, we find that $n_e(i \leqslant 11) = 2$ and $n_e(i \geqslant 291) = 0$ for $E_0 = 1$. Moreover, the surface domains with $\Delta(i) = 0$ coincide exactly with the surface insulator domains. Thus, we observe the direct surface superconductor-insulator transition without the presence of an intermediate metallic state.

To go into more detail about the behavior of the pair potential and electron distribution in the vicinity of the surface superconductor-insulator transition, we first investigate the quasiparticle energies ϵ_α and quasiparticle wave functions $u_\alpha(i)$ and $v_\alpha(i)$, as they are directly related to $n_e(i)$ and $\Delta(i)$ through Eqs. (5) and (6). Figure 2(a) shows ϵ_α as a function of α and E_0 together with the contour plot of this function. (We recall that α enumerates the quasiparticles states in an energy ascending manner.) The lowest quasiparticle energy in Fig. 2(a) corresponds to $\alpha = 1$ and $E_0 = 0$ ($\epsilon_\alpha = 0.34$), while the highest one is for $\alpha = 301$ and $E_0 = 1$ ($\epsilon_\alpha = 9.80$). We can also see that for $\alpha > 250$ the quasiparticle energies notably increase with E_0 and, moreover, this increase is much more pronounced for larger α. On the contrary, for $\alpha < 250$

the electric-field effect on ϵ_α is almost negligible. According to Fig. 2(a), all the quasiparticle states contribute to the pair potential when $E_0 \leqslant 1$ [we have $\epsilon_\alpha < \hbar\omega_D = 10$; see Eq. (6)].

The low-energy and high-energy quasiparticle wave functions $u_\alpha(i)$ and $v_\alpha(i)$ with $\alpha = 1$, 2, 300, and 301, respectively, are illustrated in Figs. 2(b)–2(e). The blue dots are the data for $E_0 = 0$, while the red stars are the results for $E_0 = 1$. Notice that $u_\alpha(i)$ and $v_\alpha(i)$ are, of course, single-value functions, and the appearance of different sets of the red and blue data in Fig. 2 is a reflection of fast oscillations of the quasiparticle wave functions from one site to another.

As mentioned above, the energies $\epsilon_{\alpha=1,2}$ are nearly constant (≈ 0.34) when E_0 increases from 0 to 1. This agrees with the fact that the corresponding quasiparticle wave functions are only slightly sensitive to the presence of the electric field. The spatial profiles of $u_{1,2}(i)$ and $v_{1,2}(i)$ for $E_0 = 0$ are in agreement with the results given in Fig. 4 of Ref. [28] and are similar to those calculated at $E_0 = 1$: the maxima of their absolute values are located at $i = 151$, while the wave functions are almost zero near the boundaries.

On the contrary, the high-energy quasiparticle wave functions with $\alpha = 300$ and 301 are significantly affected by the electric field. For example, this is immediately seen from the data shown in Fig. 2(d1). One can also see the presence of significant deviations between the blue ($E_0 = 0$) and red ($E_0 = 1$) data near the chain edges in Figs. 2(d2) and 2(e1). These deviations are the signature of the accumulation of charges at the edges of the chain in the presence of a sufficiently strong electric field. For high-energy quasiparticle states with even α we find a significant increase in $|v_\alpha(i = 1)|$, resulting from the accumulation of electrons at the left edge. For high-energy states with odd α we observe large values of $|u_\alpha(i = 301)|$ due to the concentration of positive charges at the right edge of the chain.

Now, we investigate how the quasiparticle properties are connected to changes in and suppression of the pair potential near the chain edges. To facilitate our consideration, we
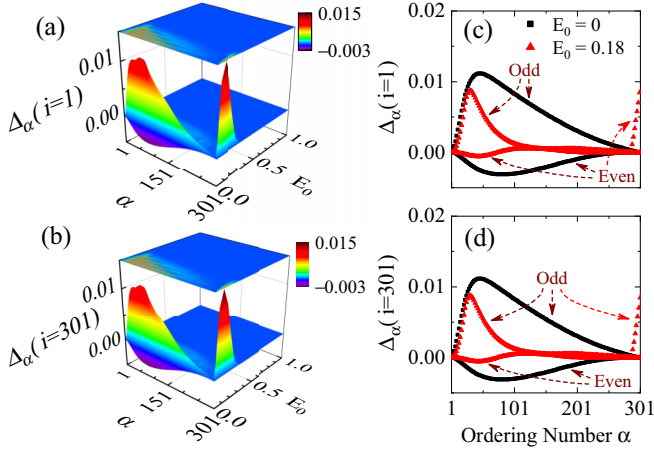
FIG. 3. (a) and (b) The single-species quasiparticle contribution to the pair potential $\Delta_\alpha(i)$ calculated for $i = 1$ and 301 as a function of α and E_0 (the upper panel is the corresponding contour plot). (c) and (d) The same quantity, but as a function of α at $E_0 = 0$ (black squares) and 0.18 (red triangles); here, the sets (branches) corresponding to odd and even values of α are displayed. The microscopic parameters are the same as in Fig. 1.

FIG. 4. The quasiparticle wave functions $u_\alpha(i)$ and $v_\alpha(i)$ versus the site number i for (a) $\alpha = 31$, (b) 44, (c) 300, and (d) 301 at $E_0 = 0.18$. The material parameters are the same as in Fig. 1.

introduce

$$\Delta_\alpha(i) = g\, u_\alpha(i) v_\alpha^*(i)[1 - 2f_\alpha], \qquad (12)$$

which is the contribution to $\Delta(i)$ of the quasiparticles related to a particular value of α. Figures 3(a) and 3(b) demonstrate $\Delta_\alpha(i)$ as a function of α and E_0 at the boundaries $i = 1$ and 301, respectively. The upper panels in Figs. 3(a) and 3(b) are the corresponding contour plots. Notice that since $\hbar\omega_D = 10$, all quasiparticles with positive energies are inside the Debye window and hence contribute to the pair potential, as seen from Fig. 2. The data given in Figs. 3(a) and 3(b) look nearly the same, but there are minor differences discussed below. For $E_0 \lesssim 0.35$, both $\Delta_\alpha(i = 1)$ and $\Delta_\alpha(i = 301)$ exhibit two pronounced maxima: one occurs in the domain of low quasiparticle energies, while the other (which is much sharper) takes place at about $\alpha \approx 301$. The data shown in Figs. 3(a) and 3(b) make it possible to conclude that for $E_0 < 0.35$ both low- and high-energy quasiparticles make significant contributions to $\Delta(i = 1, 301)$. However, for $E_0 > 0.35$ these contributions are significantly depleted, as the blue color in both panels represents nearly zero values of Δ_α.

Further details about $\Delta_\alpha(i = 1, 301)$ are given in Figs. 3(c) and 3(d), where $\Delta_\alpha(i = 1, 301)$ are shown as a function of α at $E_0 = 0$ (black squares) and $E_0 = 0.18$ (red triangles). First, we discuss the results for $E_0 = 0$. In the absence of the electric field, $\Delta_\alpha(i = 1)$ and $\Delta_\alpha(i = 301)$ exhibit two branches: positive with odd α and negative with even α. The data for $\Delta_\alpha(i = 1)$ and $\Delta_\alpha(i = 301)$ are the same, which reflects the inversion symmetry of the chain in the absence of the electric field. The fast oscillation between the positive (odd) and negative (even) values of $\Delta_\alpha(i = 1, 301)$ is related to the presence of a π-phase shift between $u_\alpha(i)$ and $v_\alpha(i)$ at the boundaries $i = 1$ and $i = 301$ [see Eq. (12) at $T = 0$]. In particular, $u_\alpha(i = 1, 301)$ and $v_\alpha(i = 1, 301)$ have the same sign for a quasiparticle with odd α, while they have opposite
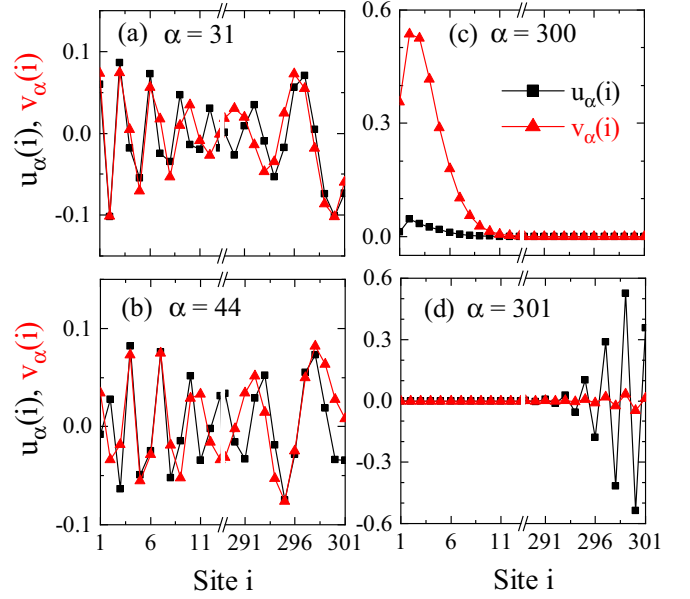
signs for even α. Similar results can be seen from Figs. 4(a) and 4(b), where $u_\alpha(i)$ and $v_\alpha(i)$ are shown for $\alpha = 31$ and 44 [here, the data are for $E_0 = 0.18$]. The maximal contribution of the positive branch for $E_0 = 0$ occurs at $\alpha = 47$, while the most pronounced but less significant (compared to the odd states) input of the negative branch is at $\alpha = 82$, which matches the slope variation of the accumulative pair potential in Fig. 3 of Ref. [30].

Now, let us consider $\Delta_\alpha(i = 1, 301)$ calculated for $E_0 = 0.18$ and also given in Figs. 3(c) and 3(d). Like in the data for zero field, we again have positive and negative branches in the dependence of $\Delta_\alpha(i = 1, 301)$ on α. Compared to the case of $E_0 = 0$, the low-energy maximum and minimum of these two branches become less pronounced, reflecting the appearance of the additional local maximum of the positive branch due to the high-energy quasiparticles. The positions of these low-energy minimum and maximum are shifted towards smaller values of α, i.e., to $\alpha = 31$ and $\alpha = 44$, respectively. For $\alpha < 150$ the positive and negative branches still correspond to odd and even α, which is the same as in the case of $E_0 = 0$. However, this correspondence is broken for high quasiparticle energies. In particular, the situation changes dramatically for $\alpha > 285$. Here, the positive branch for $i = 1$ corresponds to even α values [see Fig. 3(c)], while the positive branch for $i = 301$ is related to odd α [see Fig. 3(d)]. This is dictated by the breakdown of the inversion symmetry due to the presence of the electric field. For example, as shown in Fig. 4(c), $u_\alpha(i = 1)$ and $v_\alpha(i = 1)$ for $\alpha = 300$ are finite and positive at $i = 1$, while both wave functions are nearly zero at the other boundary, $i = 301$. This means that the contribution of the states with $\alpha = 300$ to the pair potential at $i = 301$ is nearly zero. However, the quasiparticles with $\alpha = 301$ are accumulated near $i = 301$, so that their contribution to the order parameter is depleted at $i = 1$. Thus, when the electric
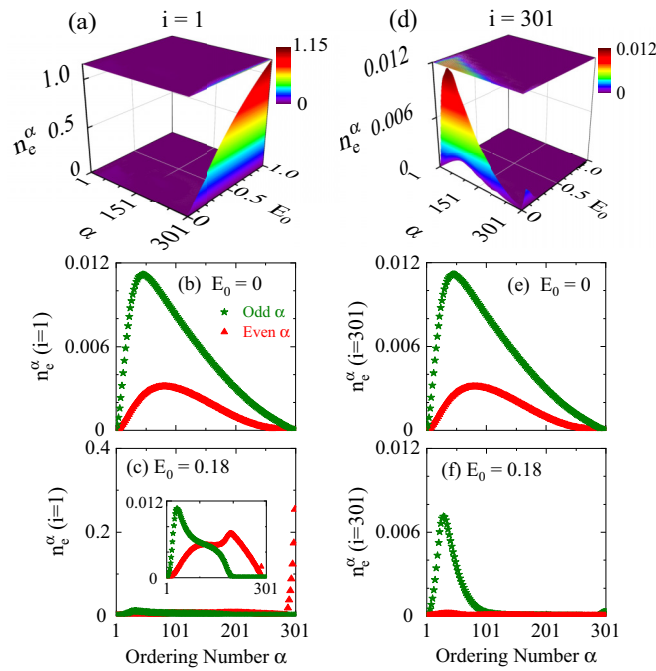
FIG. 5. (a) and (d) The single-species quasiparticle contribution to the electron density n_e^α calculated for $i = 1$ and 301, respectively, as a function of α and E_0; (b) and (e) $n_e^\alpha(i = 1, 301)$ as a function of α for $E_0 = 0$; and (c) and (f) $n_e^\alpha(i = 1, 301)$ versus α for $E_0 = 0.18$. The green stars represent odd values of α, whereas the red triangles are the data for even α. The material parameters are the same as in Fig. 1.

field is switched on, we find complex rearrangement of the quasiparticle spatial distributions, and this is related to significant depletion of the pair potential near the chain edges.

To explore the accumulation/depletion of the charge carriers at the chain edges, we consider

$$n_e^\alpha(i) = 2\{f(\epsilon_\alpha)|u_\alpha(i)|^2 + [1 - f(\epsilon_\alpha)]|v_\alpha(i)|^2\}, \quad (13)$$

which is the contribution of the quasiparticles with quantum number α to $n_e(i)$. In Figs. 5(a) and 5(d), $n_e^\alpha(i)$ is shown as a function of α and E_0 at $i = 1, 301$. For greater detail, Figs. 5(b)–5(f) demonstrate $n_e^\alpha(i)$ as a function of α, calculated for $i = 1$ and $i = 301$ at $E_0 = 0, 0.18$. The inset in Fig. 5(c) is a zoomed-in plot. The contributions of quasiparticles with odd and even α are given by green stars and red triangles, respectively.

From Fig. 5(a), we can see that $n_e^\alpha(i = 1)$ increase significantly with E_0 for high-energy quasiparticles with $\alpha > 280$. However, only low-energy quasiparticles with $\alpha \approx 50$ contribute to $n_e^\alpha(i = 301)$. Furthermore, this contribution is notable only at the fields with $E_0 < 0.35$. When E_0 exceeds 0.35, all quasiparticles produce zero contribution to $n_e(i = 301)$.

As seen from Fig. 5(b) and 5(e), the profiles of $n_e^\alpha(i = 1, 301)$ are the same in the absence for zero field (the inversion symmetry). At $E_0 = 0.18$, $n_e^\alpha(i = 1)$ for $i = 1$ differs significantly from that for $i = 301$. In particular, when E_0 increases from 0 to 0.18, the odd-α branch of $n_e^\alpha(i = 301)$ decreases significantly, so that its maximum drops from 0.011 to 0.007. At the same time the even-α branch of $n_e^\alpha(i = 301)$
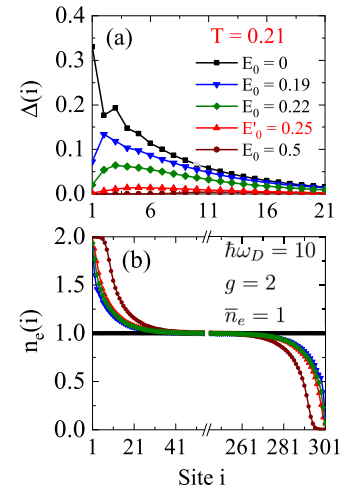
FIG. 6. (a) The spatial pair potential $\Delta(i)$ and (b) election distribution $n_e(i)$ at $T = 0.21$ with $E_0 = 0, 0.19, 0.22, 0.25$, and 0.5. The other parameters are the same as in Fig. 1. The boundary electric field E_0' corresponds to the case with $\Delta(i = 1, 301) = 0$.

approaches nearly zero. This means that $n_e(i = 301)$ exhibits a notable decrease due to the presence of an applied electric field, and we have the concentration of the positive charge near the right edge of the chain. For $n_e^\alpha(i = 1)$ we find a qualitatively different picture. Although the contributions of the quasiparticles with $\alpha < 280$ decrease with increasing E_0, the sector of high-energy states exhibits a huge increase of $n_e^\alpha(i = 1)$. As a result, $n_e(i = 1)$ increases significantly when E_0 rises from 0 to 0.18, which is clearly the reflection of the electron accumulation near the left edge of the chain due to the applied electric field.

B. Phase diagram of surface insulating states

Here, we study the phase diagram of the surface superconducting, metal (normal), and insulating states depending on the temperature T and external field E_0. To have an idea about the temperature effect on the superconductor-insulator transition, $\Delta(i)$ and $n_e(i)$ are shown in Fig. 6 for $E_0 = 0$, 0.19, 0.22, 0.25, and 0.5 at $T = 0.21$. The other parameters of the calculation are the same as in Fig. 1. As can be seen, $\Delta(i = 1)$ [and also $\Delta(i = 301)$] becomes zero when E_0 crosses the value $E_0' = 0.25$, which differs significantly from $E_0^* = 0.35$ at $T = 0$ (see Fig. 1). At the same time we find that $n_e(i = 1) = 1.94$ [while $n_e(i = 301) = 0.06$] at $E_0 = E_0'$. This means that there is no full occupation for $i = 1$ at $E_0 = E_0'$, and also, site $i = 301$ is not completely empty in this case. Thus, E_0' marks the onset of the surface normal state rather than the insulating one. The surface insulating state appears at $T = 0.21$ only when E_0 crosses the critical value $E_0^* = 0.44$. For larger fields $n_e(i = 1) = 2$, and $n_e(i = 301) = 0$, as seen in Fig. 4. Thus, at finite temperatures the electric-field-induced superconductor-insulator transition is replaced by the superconductor-metal-insulator transition. When E_0 increases at $T = 0.21$, we first find the superconducting-normal transition at $E_0 = E_0' = 0.25$ and then the metal-insulator transition at $E_0 = E_0^* = 0.44$.
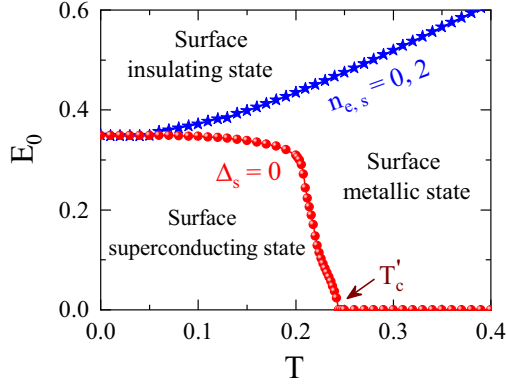
FIG. 7. The phase diagram of the surface superconductor-metal-insulator transition in the E_0-T plane. The superconducting-normal boundary is given by the curve above which $\Delta_s = \Delta(i=1, 301) = 0$. The metal-insulator boundary marks the onset of the insulating state $n_e(i=1) = 2$ and $n_e(i=301) = 0$, which is referred to as $n_{e,s} = 0, 2$.

Figure 7 shows the phase diagram in the E_0-T plane that describes the surface superconductor-metal(normal)-insulator states calculated for the 1D chain. All the material parameters are the same as in Fig. 1. The red solid circles represent the boundary between the surface superconducting and normal states above which $\Delta_s = \Delta(i=1, 301) = 0$. The blues stars yield the boundary between the metallic and insulating states. Above this boundary we have $n_e(i=1) = 2$ and $n_e(i=301) = 0$. Below the lower boundary the surface of the sample is superconducting. Above the upper boundary we have the surface insulating state. Between the boundaries the surface of the system is in the normal metallic state.

As can be seen, when the temperature increases, the critical value E_0' remains nearly the same up to $T = 0.2$. Then, it drops rapidly and becomes zero at $T_c' = 0.244$. On the other hand, E_0^*, which marks the onset of the surface insulating state, slowly increases with the temperature from 0.35 to 0.6 when the temperature goes from 0 to 0.4. This increase is due to the thermal smearing in the Fermi-Dirac distribution. We find that the lower and upper boundaries approach each other at $E_0 \approx 0.35$ for $T < 0.05$ ($\approx 20.5\% T_c'$). Thus, we can expect the direct superconductor-insulator transition to occur at $T < 0.05$. Here, we note that the zero-T critical value of E_0 is not universal. Our numerical study demonstrates that its value (in units of t/ea) depends on the microscopic parameters such as the coupling constant, the electron filling level, the Debye energy, etc. However, the qualitative features of the surface phase diagram remain unchanged.

We remark that the qualitative picture of our results for the surface transformation under the applied electric field is in qualitative agreement with the phase diagram of the superconductor-insulator transition in (Li, Fe)OHFeSe thin flakes obtained with the transport measurements [22,23]. This is especially true of the phase boundary between the superconducting and insulating states at low temperatures. In addition, our numerical results for the electric-field dependence of T_c

(i.e., the red curve in Fig. 7) are in qualitative agreement with the experimental data for 2-nm-thick $GdBa_2Cu_3O_{7-x}$ films shown in Fig. 3(a) of Ref. [11], the results for $SrTiO_3$ given in Fig. 4(a) of Ref. [18], and the data for Ti-based superconductors shown in Fig. 5(c) of Ref. [19], where T_c was found to decrease with increasing gate voltage (the strength of the electric field).

Finally, based on our results, we can estimate the strength of E_0. The data shown in Fig. 1(c) demonstrate that $\Delta_b \approx t/3 < \mu_F - \xi_s = 2t$, with Δ_b being the bulk pair potential at $i = 151$, which is beyond the strong-coupling limit (i.e., $\Delta \geqslant \mu_F - \xi_s$) [41]. As an example of the weak-coupling superconductor, we can use $SrTiO_3$. For this material we have $\Delta \approx 0.1$ meV [42], and the average lattice constant $a \approx 4$ Å [43]. Then, we find $t/(ea) = 7.5 \times 10^5$ V/m, where the above relation between Δ_b and t is utilized. Therefore, the transition electric field from the surface superconducting state to the surface insulating state at $T = 0$ is estimated as $E_0^* = 0.35 t/(ea) = 2.6 \times 10^5$ V/m, which is two orders of magnitude lower than the dielectric breakdown field (3.1×10^7 V/m) of $SrTiO_3$ films [44]. For superconductors with $\Delta = 10$ meV, keeping $a \approx 4$ Å and the same relation between Δ_b and t, we have $E_0^* = 2.6 \times 10^7$ V/m. This electric field is also available in experiments [19]. Even fields of the order of 10^{10} V/m can be achieved based on the voltage-induced polarization of an electrolyte [45].

IV. CONCLUSIONS

In conclusion, the electric-field-induced surface insulating state was revealed in a superconductor by numerically solving the Bogoliubov–de Gennes equations for the one-dimensional attractive Hubbard model in a self-consistent manner. We found that the surface insulating state appears once the chain sites near the edges are either fully occupied by electrons or completely empty. This rearrangement occurs due to the applied electric field, affecting the electron distribution near the surface and suppressing the surface pair potential. At zero temperature we found the superconductor-insulator phase transition arises with increasing electric field. At finite temperatures the system first undergoes the surface superconductor-metal transition and then, at larger fields, the metal-insulator phase transition. The phase diagram of the surface superconducting, metallic, and insulating states is obtained for a wide range of the temperatures and applied electric fields. Remarkably, this diagram qualitatively matches the results of the transport measurements in (Li, Fe)OHFeSe thin flakes [22,23].

[1] R. E. Glover and M. D. Sherrill, Changes in Superconducting Critical Temperature Produced by Electrostatic Charging, Phys. Rev. Lett. **5**, 248 (1960).

[2] G. Bonfiglioli, R. Malvano, and B. B. Goodman, Search for an effect of surface charging on the superconducting transition temperature of tin films, J. Appl. Phys. **33**, 2564 (1962).

[3] H. Meissner, Search for surface superconductivity induced by an electric field, Phys. Rev. **154**, 422 (1967).

[4] I. Golokolenov, A. Guthrie, S. Kafanov, Y. A. Pashkin, and V. Tsepelin, On the origin of the controversial electrostatic field effect in superconductors, Nat. Commun. **12**, 2747 (2021).

[5] T. Elalaily, O. Kürtössy, Z. Scherübl, M. Berke, G. Fülöp, I. E. Lukács, T. Kanne, J. Nygård, K. Watanabe, T. Taniguchi, P. Makk, and S. Csonka, Gate-controlled supercurrent in epitaxial Al/InAs nanowires, Nano Lett. **21**, 9684 (2021).

[6] P. Solinas, A. Amoretti, and F. Giazotto, Sauter-Schwinger Effect in a Bardeen-Cooper-Schrieffer Superconductor, Phys. Rev. Lett. **126**, 117001 (2021).

[7] A. Amoretti, Superconductors in strong electric fields: Quantum Electrodynamics meets Superconductivity, J. Phys.: Conf. Ser. **2531**, 012001 (2023).

[8] N. E. Staley, J. Wu, P. Eklund, Y. Liu, L. Li, and Z. Xu, Electric field effect on superconductivity in atomically thin flakes of NbSe$_2$, Phys. Rev. B **80**, 184505 (2009).

[9] Y. Mizohata, M. Ichioka, and K. Machida, Multiple-gap structure in electric-field-induced surface superconductivity, Phys. Rev. B **87**, 014505 (2013).

[10] C. H. Ahn, S. Gariglio, P. Paruch, T. Tybell, L. Antognazza, and J.-M. Triscone, Electrostatic modulation of superconductivity in ultrathin GdBa$_2$Cu$_3$O$_{7-x}$ films, Science **284**, 1152 (1999).

[11] C. H. Ahn, J.-M. Triscone, and J. Mannhart, Electric field effect in correlated oxide systems, Nature (London) **424**, 1015 (2003).

[12] K. S. Takahashi, D. Matthey, D. Jaccard, J.-M. Triscone, K. Shibuya, T. Ohnishi, and M. Lippmaa, Electrostatic modulation of the electronic properties of Nb-doped SrTiO$_3$ superconducting films, Appl. Phys. Lett. **84**, 1722 (2004).

[13] P. Orús, V. M. Fomin, J. M. De Teresa, and R. Córdoba, Critical current modulation induced by an electric field in superconducting tungsten-carbon nanowires, Sci. Rep. **11**, 17698 (2021).

[14] F. Paolucci, F. Crisá, G. De Simoni, L. Bours, C. Puglia, E. Strambini, S. Roddaro, and F. Giazotto, Electrostatic field-driven supercurrent suppression in ionic gated metallic superconducting nanotransistors, Nano Lett. **21**, 10309 (2021).

[15] M. F. Ritter, A. Fuhrer, D. Z. Haxell, S. Hart, P. Gumann, H. Riel, and F. Nichele, A superconducting switch actuated by injection of high-energy electrons, Nat. Commun. **12**, 1266 (2021).

[16] A. Amoretti, D. K. Brattan, N. Magnoli, L. Martinoia, I. Matthaiakakis, and P. Solinas, Destroying superconductivity superconductivity in thin films with an electric field, Phys. Rev. Res. **4**, 033211 (2022).

[17] K. A. Parendo, K. H. S. B. Tan, A. Bhattacharya, M. Eblen-Zayas, N. E. Staley, and A. M. Goldman, Electrostatic Tuning of the Superconductor-Insulator Transition in Two Dimensions, Phys. Rev. Lett. **94**, 197004 (2005).

[18] K. Ueno, S. Nakamura, H. Shimotani, A. Ohtomo, N. Kimura, T. Nojima, H. Aoki, Y. Iwasa, and M. Kawasaki, Electric-field-induced superconductivity in an insulator, Nat. Mater. **7**, 855 (2008).

[19] F. Paolucci, G. De Simoni, P. Solinas, E. Strambini, N. Ligato, P. Virtanen, A. Braggio, and F. Giazotto, Magnetotransport Experiments on Fully Metallic Superconducting Dayem-Bridge Field-Effect Transistors, Phys. Rev. Appl. **11**, 024061 (2019).

[20] J. T. Ye, S. Inoue, K. Kobayashi, Y. Kasahara, H. T. Yuan, H. Shimotani, and Y. Iwasa, Liquid-gated interface superconductivity on an atomically flat film, Nat. Mater. **9**, 125 (2010).

[21] A. T. Bollinger, G. Dubuis, J. Yoon, D. Pavuna, J. Misewich, and I. Bozović, Superconductor-insulator transition in La$_{2-x}$Sr$_x$CuO$_4$ at the pair quantum resistance, Nature (London) **472**, 458 (2011).

[22] L. Ma, B. Lei, N. Wang, K. Yang, D. Liu, F. Meng, C. Shang, Z. Sun, J. Cui, C. Zhu, T. Wu, Z. Sun, L. Zou, and X. Chen, Electric-field-controlled superconductor-ferromagnetic insulator Transition, Sci. Bull. **64**, 653 (2019).

[23] R. Yin, L. Ma, Z. Wang, C. Ma, X. Chen, and B. Wang, Reversible superconductor-insulator transition in (Li, Fe)OHFeSe flakes visualized by gate-tunable scanning tunneling spectroscopy, ACS Nano **14**, 7513 (2020).

[24] K. Tanaka and F. Marsiglio, Anderson prescription for surfaces and impurities, Phys. Rev. B **62**, 5345 (2000).

[25] K. Takasan and M. Sato, Control of magnetic and topological orders with a DC electric field, Phys. Rev. B **100**, 060408(R) (2019).

[26] P. G. de Gennes, *Superconductivity of Metals and Alloys* (Benjamin, New York, 1966).

[27] A. Samoilenka, M. Barkman, A. Benfenati, and E. Babaev, Pair-density-wave superconductivity of faces, edges, and vertices in systems with imbalanced fermions, Phys. Rev. B **101**, 054506 (2020).

[28] M. D. Croitoru, A. A. Shanenko, Y. Chen, A. Vagov, and J. A. Aguiar, Microscopic description of surface superconductivity, Phys. Rev. B **102**, 054513 (2020).

[29] L. Chen, Y. Chen, W. Zhang, and S. Zhou, Non-gapless excitation and zero-bias fast oscillations in the LDOS of surface superconducting states, Phys. B (Amsterdam, Neth.) **646**, 414302 (2022).

[30] Y. Bai, Y. Chen, M. D. Croitoru, A. A. Shanenko, X. Luo, and Y. Zhang, Interference-induced surface superconductivity: Enhancement by tuning the Debye energy, Phys. Rev. B **107**, 024510 (2023).

[31] A. A. Shanenko, M. D. Croitoru, R. G. Mints, and F. M. Peeters, New Andreev-Type States in Superconducting Nanowires, Phys. Rev. Lett. **99**, 067007 (2007).

[32] Y. Chen, Q. Zhu, Q. Liu, and Q. Ren, Nanoscale superconductors: Dual Friedel oscillations of single quasiparticles and corresponding in influence on determination of the gap energy, Phys. B (Amsterdam, Neth.) **545**, 458 (2018).

[33] Y. Chen, M. D. Croitoru, A. A. Shanenko, and F. M. Peeters, Superconducting nanowires: Quantum confinement and spatially dependent Hartree-Fock potential, J. Phys.: Condens. Matter **21**, 435701 (2009).

[34] P. G. de Gennes, Boundary effects in superconductors, Rev. Mod. Phys. **36**, 225 (1964).

[35] K. Szałowski, Electric field control of the indirect magnetic coupling through a short graphene nanoribbon, Phys. Rev. B **90**, 085410 (2014).

[36] J. Mannhart, J. G. Bednorz, K. A. Muller, and D. G. Schlom, Electric field effect on superconducting YBa$_2$Cu$_3$O$_{7-\delta}$ films, Z. Phys. B **83**, 307 (1991).

[37] P. Konsin and B. Sorkin, Electric field effects in high-T_c cuprates, Phys. Rev. B **58**, 5795 (1998).

[38] X. Xi, C. Doughty, A. Walkenhorst, C. Kwon, Q. Li, and T. Venkatesan, Effects of Field-Induced Hole-Density Modulation on Normal-State and Superconducting Transport in YBa$_2$Cu$_3$O$_{7-\delta}$, Phys. Rev. Lett. **68**, 1240 (1992).

[39] M. Konishi, K. Hayashi, A. Odagawa, Y. Enomoto, Y. Yamada, M. Nakamura, K. Ohtsu, Y. Kanamori, M. Tagami, S. Koyama, and Y. Shiohara, *Homo-epitaxial Growth of YBCO Thin Film on YBCO Single Crystal*, Advances in Superconductivity Vol. 6 (Springer, Tokyo, 1994).

[40] F. Carillo, G. Papari, D. Stornaiuolo, D. Born, D. Montemurro, P. Pingue, F. Beltram, and F. Tafuri, Little-Parks effect in single nanoscale YBa$_2$Cu$_3$O$_{6+x}$ rings, Phys. Rev. B **81**, 054505 (2010).

[41] K. Okazaki, Y. Ito, Y. Ota, Y. Kotani, T. Shimojima, T. Kiss, S. Watanabe, C.-T. Chen, S. Niitaka, T. Hanaguri, H. Takagi, A. Chainani, and S. Shin, Superconductivity in an electron band just above the Fermi level: Possible route to BCS-BEC superconductivity, Sci. Rep. **4**, 4109 (2014).

[42] K. Ahadi, L. Galletti, Y. Li, S. Salmani-Rezaie, W. Wu, and S. Stemmer, Enhancing superconductivity in SrTiO$_3$ films with strain, Sci. Adv. **5**, eaaw0120 (2019).

[43] N. Ohama, H. Sakashita, and A. Okazaki, The temperature dependence of the lattice constant of SrTiO$_3$ around the 105 K transition, Phase Transitions **4**, 81 (1984).

[44] Z. Wang, V. Kugler, U. Helmersson, N. Konofaos, E. K. Evangelou, S. Nakao, and P. Jin, Electrical properties of SrTiO$_3$ thin films on Si deposited by magnetron sputtering at low temperature, Appl. Phys. Lett. **79**, 1513 (2001).

[45] A. S. Dhoot, J. D. Yuen, M. Heeney, I. McCulloch, D. Moses, and A. J. Heeger, Beyond the metal-insulator transition in polymer electrolyte gated polymer field-effect transistors, Proc. Natl. Acad. Sci. USA **103**, 11834 (2006).